Redox Biology 86 (2025) 103834

Contents lists available at ScienceDirect

Redox Biology

journal homepage: www.elsevier.com/locate/redox

Oxidative stress-induced ZEB1 acetylation drives a hybrid epithelial-mesenchymal phenotype and promotes lung metastasis in triple-negative breast cancer

Min Guo [a,b], Yan-Jing Wang [a], Jie Shi [a], Li-Xia Cao [a], Yang Ou [a], Xiao Jia [c], Chun-Chun Qi [a], Zhao-Xian Li [a], Yu-Xin Liu [a], Si-Yu Zuo [a], Qiu-Ying Shuai [a], Tian-Wen Yu [a], Hua-Yu Hu [a], Xiao Chen [a], Meng-Dan Feng [a], Yao Xue [a], Hang Wang [a], Pei-Qing Sun [d], Lei Liu [e,*], Yi Shi [a,**], Shuang Yang [a,***]

[a] Tianjin Key Laboratory of Tumour Microenvironment and Neurovascular Regulation, School of Medicine, Nankai University, Tianjin, 300071, PR China
[b] Department of Clinical Laboratory, Tianjin Union Medical Center of Nankai University, Tianjin, 300121, PR China
[c] State Key Laboratory of Medicinal Chemical Biology, College of Pharmacy and Tianjin Key Laboratory of Molecular Drug Research, Nankai University, Tianjin, 300000, PR China
[d] Department of Cancer Biology, Wake Forest University School of Medicine, Winston-Salem, NC, 27157, USA
[e] Tianjin Medical University Cancer Institute & Hospital, Tianjin, 300071, PR China

ARTICLE INFO

Keywords:
Oxidative stress
ZEB1
Acetylation
Hybrid epithelial-mesenchymal phenotype
Lung metastasis
TNBC

ABSTRACT

While epithelial-mesenchymal plasticity (EMP) drives cancer metastasis, its regulation by redox dynamics remains poorly understood. Herein, we identified an oxidative stress-responsive CBP/SIRT1 axis that coordinated ZEB1 acetylation at K1108 to promote lung metastasis in triple-negative breast cancer (TNBC). Mechanistically, the biochemical and functional analyses revealed that the dual-acetyltransferase CBP, through stabilization and autoacetylation by oxidative stress, formed a dynamic partnership with SIRT1 to execute precision lysine modification. This post-translational rheostat triggered the functional metamorphosis of ZEB1. During this process, ZEB1 dissociation from the transcriptional corepressor CtBP, while recruiting CBP, converts ZEB1 into a transcriptional activator of epithelial genes. The resulting hybrid epithelial–mesenchymal phenotype orchestrated dual metastatic competence-maintaining stromal interaction capacity through partial epithelial–mesenchymal transition (EMT) while establishing NADPH-driven redox supremacy to circumvent ferroptosis. Importantly, this acetyl switch of ZEB1 revealed a metastasis-specific therapeutic vulnerability in TNBC. Our work thus highlighted ZEB1 acetylation as a redox-interpreted mechanism coupling phenotypic plasticity with stress resistance, proposing targeted disruption of this protein post-translational modification (PTM) circuit as a precision strategy against metastatic progression.

1. Introduction

Breast cancer is the most common malignancy in women worldwide, accounting for 25 % of new cancer cases and 16 % of cancer-related deaths in women [1]. Notably, patients with distant metastasis, especially those with triple-negative breast cancer (TNBC), have a relatively poor prognosis [2]. Therefore, elucidation of the molecular mechanisms underlying lethal metastasis is urgently needed to develop new and effective treatments for breast cancer.

Epithelial-mesenchymal plasticity (EMP) refers to the dynamic transitions between epithelial and mesenchymal states of tumour cells and is linked to various malignant behaviours, such as migration, invasion, and distant metastasis [3]. In primary tumours, epithelial-mesenchymal transition (EMT) is associated with a reduction in the expression of epithelial markers, such as E-cadherin. However, recent studies have shown that for metastatic colonization of distant

* Corresponding author.
** Corresponding author. School of Medicine, Nankai University, Tianjin, 300071, PR China.
*** Corresponding author. School of Medicine, Nankai University, Tianjin, 300071, PR China.
E-mail addresses: liuleidoc@126.com (L. Liu), yishi@nankai.edu.cn (Y. Shi), yangshuang@nankai.edu.cn (S. Yang).

https://doi.org/10.1016/j.redox.2025.103834
Received 22 July 2025; Received in revised form 15 August 2025; Accepted 18 August 2025
Available online 19 August 2025
2213-2317/© 2025 The Authors. Published by Elsevier B.V. This is an open access article under the CC BY-NC-ND license (http://creativecommons.org/licenses/by-nc-nd/4.0/).

organs, tumour cells need to re-express E-cadherin and adopt a hybrid epithelial-mesenchymal phenotype [3,4]. For example, Padmanaban et al. showed that most large lung metastases derived from PyMT breast tumours are E-cadherin-positive, based on lineage tracing analysis [5]. Similarly, Cui et al. reported that the impaired function of MLL3, a histone methyltransferase, induces breast cancer cells to acquire a hybrid epithelial-mesenchymal phenotype, promoting their metastatic colonization of the lung [6]. Furthermore, circulating tumour cells with high metastatic potential also exhibit a hybrid epithelial-mesenchymal phenotype [4,7]. Notably, this subpopulation of cells exhibits increased resistance to apoptosis under oxidative stress conditions [8]. While EMP confers survival advantages to tumour cells, the stimuli and molecular mechanisms driving the acquisition of this hybrid phenotype within the complex tumour microenvironment remain largely unclear.

In TNBC, ZEB1, as a core transcription factor involved in EMT, is highly expressed and associated with distant tumour metastasis [9–14]. During this process, ZEB1 expression is significantly upregulated in primary breast tumours compared to normal mammary tissue. However, recent studies suggest that ZEB1 levels remain relatively stable between primary and metastatic lesions, suggesting that the possible mechanism might involve post-translational modifications (PTMs) of the protein. Of note, acetylation is one of the most common PTMs that allows tumour cells to respond rapidly to metabolic and microenvironmental stimuli during tumour initiation and progression [15,16]. For example, previous report has shown that p300 and PCAF form a complex with ZEB1 and lead to its lysine acetylation, which subsequently alleviates the transcriptional repression of E-cadherin [17]. Therefore, further investigations are needed to determine the precise ZEB1 acetylation site and underlying regulatory mechanism, especially those involved in the acquisition of a hybrid epithelial-mesenchymal phenotype in distant metastasis.

In this study, we discovered that oxidative stress increased ZEB1 acetylation during metastatic colonization of the lung in TNBC by driving a hybrid epithelial-mesenchymal phenotype. This process enhanced the plasticity of tumour cells, enabling them to counteract oxidative damage-induced ferroptosis during distant metastasis. We also elucidated the critical biological function of ZEB1^{K1108} acetylation and identified CBP and SIRT1 as the key regulatory enzymes in the oxidative stress response. Our results together revealed that acetylated ZEB1 switched binding cofactors from the corepressor CtBP to the coactivator CBP, thereby triggering the hybrid epithelial-mesenchymal phenotype of TNBC cells to facilitate their distant metastasis.

2. Results

2.1. Acetylated ZEB1 is upregulated in lung metastases of TNBC

Previous studies have linked elevated ZEB1 expression to a poor prognosis in TNBC patients with metastatic potential [18]. However, comparative analysis of two highly metastatic breast cancer datasets (GSE138139 and GSE2603) revealed no significant differences in ZEB1 transcript levels between primary tumours and lung metastases (Fig. S1A–C). Given the significant impact of ZEB1 on tumour metastasis, we postulated that PTMs might play a role in fine-tuning the

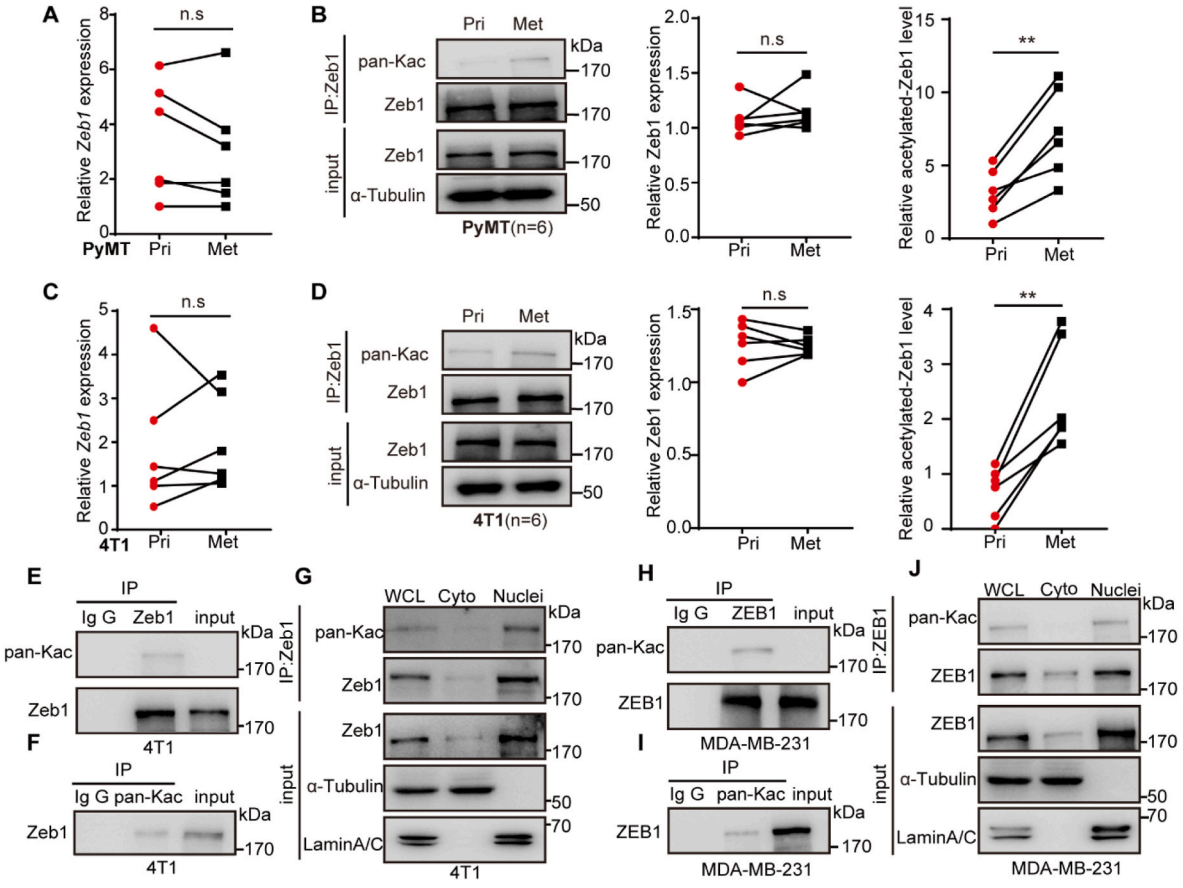

Fig. 1. Acetylated ZEB1 is upregulated in lung metastases of TNBC. (A, B) Relative mRNA (A) and protein (B) levels of Zeb1 in primary tumours and lung metastases from PyMT mice (n = 6). **(C, D)** Relative mRNA (C) and protein (D) levels of Zeb1 in primary tumours and lung metastases from the 4T1 orthotopic metastasis model (n = 6). **(E–J)** Immunoblotting (IB) and immunoprecipitation (IP) assays with anti-Zeb1 and anti-pan-Kac antibodies in 4T1 (E, F). IgG was used as a negative control. WCL, cytosolic, and nuclear fractions from 4T1 were collected for IB analysis with an anti-pan-Kac antibody (G). MDA-MB-231 cells were under the same treatments (H–J). The data are presented as the means ± SDs. Two-tailed Student's paired *t*-test was used.

function of ZEB1, even when its expression levels remain constant.

To test this hypothesis, an MMTV-PyMT spontaneous breast cancer mouse model was used, and the primary tumours and lung metastases were harvested from 15-week-old female mice (Fig. S1D). As shown in Fig. 1A and B, the mRNA and protein levels of Zeb1 did not significantly differ between the primary tumours and lung metastases. However, we observed that the pan-acetylation level of Zeb1 was markedly increased in lung metastases than that in primary tumours. Similarly, in an orthotopic tumour metastasis model with 4T1 mouse breast cancer cells (Fig. S1E), we also demonstrated that the pan-acetylation level of Zeb1 was strongly increased in lung metastases; however, the alterations in the mRNA and protein levels of Zeb1 were not as evident (Fig. 1C and D).

At the cellular level, we confirmed that ZEB1 underwent protein acetylation predominantly in the nuclear fraction of 4T1 cells (Fig. 1E–G). These results were also confirmed in MDA-MB-231 (Fig. 1H–J) and SUM-159 (Fig. S1F–H) human breast cancer cells.

2.2. CBP is the major acetyltransferase for ZEB1 acetylation

To identify the acetyltransferase that potentially regulates ZEB1 acetylation, we co-transfected V5-tagged ZEB1 with a panel of HA-tagged acetyltransferases, including p300, CBP, PCAF, HMOF, and TIP60, into HEK-293T cells. The results revealed that only CBP significantly increased the acetylation of ZEB1 (Fig. 2A), and Co-IP analysis indicated that ZEB1 physically interacted with CBP in MDA-MB-231 cells (Fig. 2B and C). Moreover, nuclear and cytoplasmic fractionation combined with IF revealed that ZEB1 and CBP predominantly colocalized in the nuclei of MDA-MB-231 cells (Fig. 2D and E). We also performed these experiments in SUM-159 cells and obtained the same results (Fig. S2A–D). Furthermore, we observed that CBP increased the acetylation of ZEB1 in a dose-dependent manner (Fig. 2F). On the contrary, specific interference with CBP decreased the acetylation level of ZEB1 in MDA-MB-231 cells (Fig. 2G), and addition of the CBP catalytic inhibitor A485 performed a similar effect (Fig. 2H). Consistently, these observations were also confirmed in SUM-159 cells (Fig. S2E and S2F). Next, to determine whether the acetylation of ZEB1 is dependent on the catalytic activity of CBP, we co-expressed ZEB1 with the wild-type CBP or catalytically inactive mutant CBP-Y1503F. The results showed that only the wild-type CBP acetylated ZEB1, whereas the mutant CBP-Y1503F did not (Fig. S2G). In addition, three truncated mutants of ZEB1 were established in HEK-293T cells (Fig. 2I) [19]. The results of Co-IP experiments demonstrated that CBP interacted with both full-length ZEB1 and its NZF and CZF domains (Fig. 2I). Similarly, MBP pulldown analysis verified that both the NZF and CZF domains could bind to CBP *in vitro* (Fig. 2J). However, only the CZF domain, but not the NZF domain, was primarily acetylated by CBP (Fig. 2K). These observations suggested that the acetyltransferase CBP could interact with the CZF domain of ZEB1 and consequently perform its acetylation.

2.3. SIRT1 specifically deacetylates ZEB1

Considering that lysine acetylation is a dynamic process that can be reversed by specific deacetylases, we sought to identify the specific deacetylase for ZEB1. For this purpose, we co-expressed ZEB1 and CBP in HEK-293T cells, followed by treatment with the deacetylase inhibitors trichostatin A (TSA) and nicotinamide (NAM), which target histone deacetylases (HDACs) and sirtuins (SIRTs), respectively. Co-IP analysis revealed that only NAM addition increased CBP-mediated ZEB1 acetylation, whereas the effect of TSA was not as evident (Fig. 3A). The same results were also observed in both MDA-MB-231 (Fig. 3B) and SUM-159 cells (Fig. S3A). Given that acetylated ZEB1 is located mainly in the nuclear, we focused on its interactions with nuclear SIRT family members, including SIRT1, SIRT2, SIRT6, and SIRT7 [20]. The results revealed that only SIRT1 was essential for both physical interaction with ZEB1 and its deacetylation in HEK-293T cells (Fig. 3C). Similarly, we validated the interaction between ZEB1 and SIRT1 in MDA-MB-231 cells (Fig. 3D and E). In addition, the results of nuclear and cytoplasmic fractionation in combination with IF staining revealed colocalization of ZEB1 and SIRT1 in the nuclei of MDA-MB-231 cells (Fig. 3F and G). These experiments were also performed in SUM-159 cells, and the same results were obtained (Fig. S3B–E). Notably, SIRT1 reduced the acetylation of ZEB1 in a dose-dependent manner (Fig. 3H), whereas the specific knockdown of SIRT1 led to increased ZEB1 acetylation in MDA-MB-231 cells (Fig. 3I). Treatment with the selective SIRT1 inhibitor EX-527 also increased the acetylation level in MDA-MB-231 cells (Fig. 3J). Similar results were obtained in SUM-159 cells (Fig. S3F and S3G).

We then co-expressed ZEB1 with the wild-type SIRT1 or its deacetylase-inactive mutant SIRT1-H363Y in HEK-293T cells, which revealed that only the wild-type SIRT1, but not SIRT1-H363Y, was able to deacetylate ZEB1 (Fig. S3H). Additionally, we found that SIRT1 specifically counteracts the effect of CBP on ZEB1 acetylation in HEK-293T cells (Fig. S3I). Moreover, we identified that SIRT1 could bind to full-length ZEB1 and its NZF and CZF domains (Fig. 3K). Consistent with these findings, the results of MBP pulldown assay confirmed that the NZF and CZF domains of ZEB1 were able to directly interact with SIRT1 *in vitro* (Fig. 3L). As expected, SIRT1 influenced only acetylation of the CZF domain (Fig. 3M). These results together suggested that SIRT1 functions as a *bona fide* deacetylase for ZEB1, which performs deacetylation by interacting with the CZF domain of ZEB1.

2.4. K1108 is a critical site for ZEB1 acetylation

To further identify the specific acetylation sites in ZEB1, HEK-293T cells were co-transfected with ZEB1 and CBP (Fig. 4A). The analysis of LC-MS/MS identified a total of 16 acetylation sites in ZEB1 (Table S1), six of which were located within its CZF domain. Subsequently, we constructed a series of acetylation-inactivated ZEB1 mutants, including CZF^{K833R}, CZF^{K929R}, CZF^{3KR} (with simultaneous mutations in the K958, K964, and K967 sites), and CZF^{K1108R}, and respectively co-expressed these mutants with CBP in HEK-293T cells. As shown in Fig. 4B, the K1108R mutation specifically reduced ZEB1 acetylation by CBP. Importantly, this acetylation site is conserved across species (Fig. 4C). Thus, a specific antibody, hereafter referred to as Ac-ZEB1, was generated to recognize ZEB1 acetylated at K1108 (Table S2). Furthermore, the expression of wild-type ZEB1 (named $shZEB1/231^{WT}$, can undergo authentic dynamic acetylation) and its inactive mutant $ZEB1^{K1108R}$ (named $shZEB1/231^{K1108R}$, acetylation-mimetic inactive mutan) were reconstituted in MDA-MB-231 cells with a specific knockdown of endogenous ZEB1 (named shZEB1/231), as shown in Fig. S4A and S4C. The Ac-ZEB1 antibody recognized the acetylated wild-type ZEB1 but not the $ZEB1^{K1108R}$ mutant (Fig. 4D). These experiments were also performed in SUM-159 cells, and the same results were obtained (Fig. S4B and S4F). Furthermore, we confirmed that CBP specifically promoted acetylation of the wild-type ZEB1 at K1108 site in HEK-293T cells (Fig. 4E), and the same results were also observed in both MDA-MB-231 (Fig. 4F) and SUM-159 (Fig. S4G) cells. Notably, the $ZEB1^{K1108R}$ mutant significantly abolished the acetylation of ZEB1 in HEK-293T cells with either gain- (Fig. 4G) or loss-of-function of CBP (Fig. S4H). As expected, SIRT1 had the opposite effect to promote deacetylation of the wild-type ZEB1 at K1108 site (Fig. 4H and I and Figure S4I); importantly, these effects were abolished in the $ZEB1^{K1108R}$ mutant, regardless of overexpression (Fig. 4J) or knockdown of SIRT1 (Fig. S4J).

Sequence alignment analysis revealed that the K1108 site in human ZEB1 corresponded to that of K1094 site in mouse Zeb1. Thus, expression of the wild-type Zeb1 (named $shZeb1/4T1^{WT}$) and its mutant $Zeb1^{K1094R}$ (named $shZeb1/4T1^{K1094R}$) was respectively reconstituted in 4T1 cells with a knockdown of endogenous Zeb1 (named shZeb1/4T1), as shown in Fig. S4D and S4E. In addition, the Ac-ZEB1 antibody specifically recognized Zeb1 that was acetylated at K1094 site (Fig. S4K)

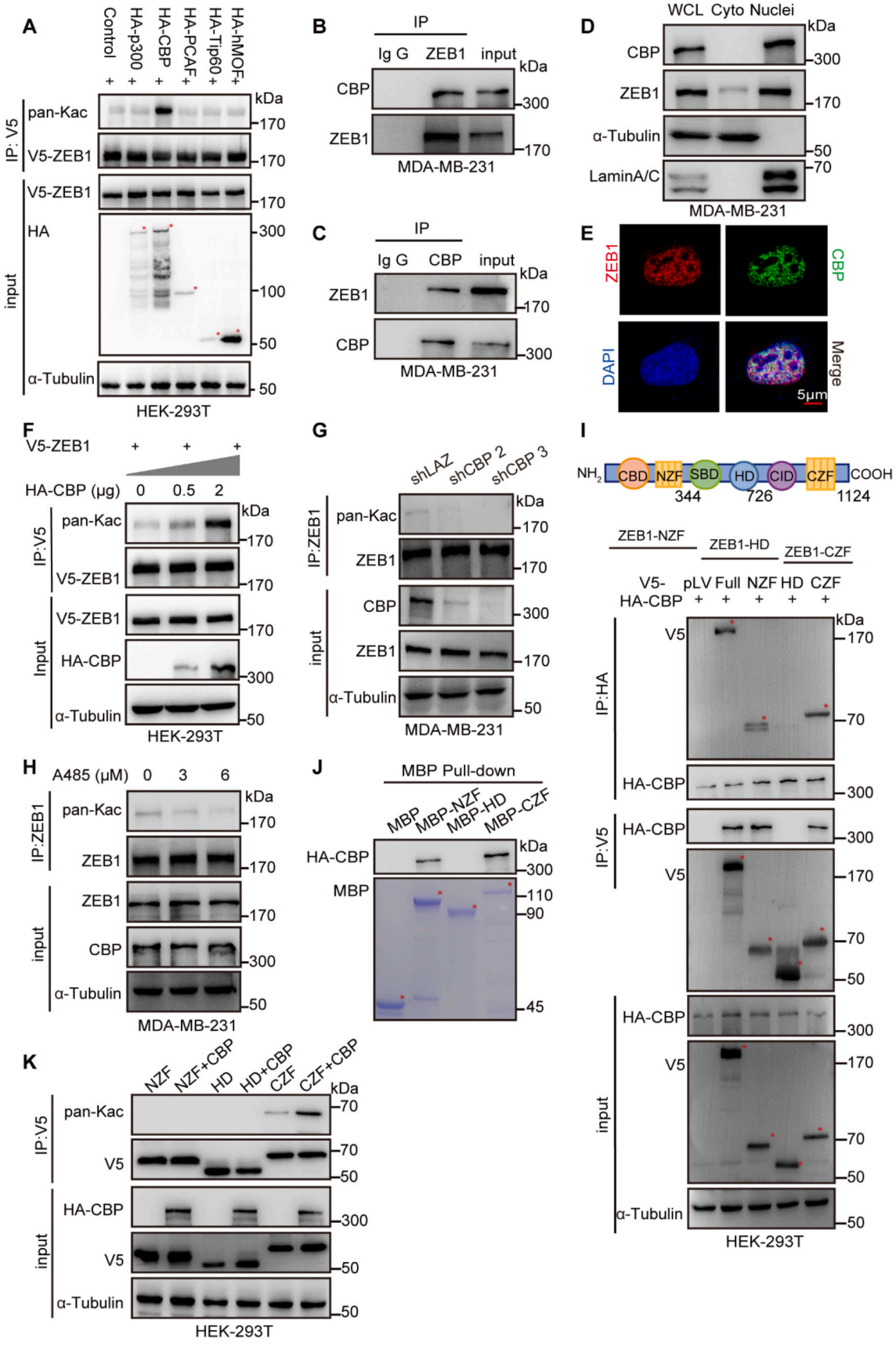

(caption on next page)

Fig. 2. CBP is the major acetyltransferase for ZEB1 acetylation. (A) IB analysis with an anti-pan-Kac antibody in HEK-293T cells co-transfected with V5-ZEB1 and the indicated HA-tagged acetyltransferases. **(B, C)** Endogenous Co-IP assays of the interaction between ZEB1 and CBP in MDA-MB-231 cells. **(D)** IB analysis of CBP and ZEB1 in the WCL, cytosolic, and nuclear fractions of MDA-MB-231 cells. **(E)** Representative IF images of MDA-MB-231 cells stained with anti-ZEB1 and anti-CBP antibodies. Scale bars, 5 μm. **(F)** IB analysis with an anti-pan-Kac antibody in HEK-293T cells co-transfected with V5-ZEB1 and different doses of HA-CBP. **(G)** IB analysis of pan-Kac levels in MDA-MB-231 cells transduced with shRNAs against CBP. **(H)** IB analysis with an anti-pan-Kac antibody in MDA-MB-231 cells by treatment with different concentrations of A485 for 6 h. **(I)** IB analysis of HEK-293T cells co-transfected with HA-CBP and V5-tagged ZEB1 truncation mutants. The model diagram of the ZEB1 domain is shown in the top panel. **(J)** MBP pulldown assays in HEK-293T cells transfected with HA-CBP. Purified MBP-ZEB1-truncated fusion proteins were identified via Coomassie blue staining. **(K)** IB analysis with an anti-pan-Kac antibody in HEK-293T cells co-transfected with V5-tagged ZEB1 truncation mutants in the presence or absence of HA-CBP.

and its levels were modulated by both Cbp (Fig. S4L) and Sirt1 (Fig. S4M).

2.5. Acetylation of ZEB1^{K1108} switches the transcriptional regulation mode of ZEB1

Next, to investigate the functional phenotypes associated with ZEB1^{K1108} acetylation, we established the constitutively active mutant ZEB1^{K1108Q}, named shZEB1/231^{K1108Q}, in shZEB1/231 cells (Fig. S4C). However, nuclear and cytoplasmic fractionation combined with IF staining revealed that acetylation at K1108 did not affect the subcellular localization of ZEB1 in shZEB1/231^{WT}, shZEB1/231^{K1108R} or shZEB1/231^{K1108Q} cells (Fig. S5A and S5B). Furthermore, a cycloheximide (CHX) chase assay demonstrated that K1108 acetylation did not influence ZEB1 protein degradation or stability (Fig. S5C and S5D). These findings were also confirmed in SUM-159 cells (Fig. S5E–H). Consistent with the previous notion that ZEB1 functions as a master EMT-related transcription factor in cancer development, we found that the expression of E-cadherin was upregulated by specifically targeting ZEB1 in MDA-MB-231 cells (Fig. 5A). Importantly, this effect was significantly weakened by reconstitution of either the wild-type ZEB1 or ZEB1^{K1108R} mutant but not by that of the ZEB1^{K1108Q} mutant. In contrast, alterations in the mesenchymal markers N-cadherin and Vimentin were not as evident. We also performed a dual-luciferase reporter assay with the −178/+92 E-cadherin promoter (Fig. 5B), which confirmed that the specific acetylation of ZEB1^{K1108} might trigger the switch of ZEB1 to a transcriptional activator for E-cadherin. Similar results were also observed in SUM-159 cells (Fig. S5I and 5J). To further verify the transcriptional regulation mode associated with ZEB1^{K1108} acetylation, we performed RNA sequencing analysis in shZEB1/231, shZEB1/231^{K1108R} and shZEB1/231^{K1108Q} cells. The results of GSEA confirmed that alterations in the acetylation of ZEB1^{K1108} were strongly associated with the EMT process (Fig. 5C). Specifically, compared with shZEB1/231 cells, shZEB1/231^{K1108R} cells presented a classical mesenchymal phenotype (Fig. 5D and E), whereas shZEB1/231^{K1108Q} cells presented a hybrid epithelial-mesenchymal phenotype (Fig. 5F and G). A direct comparison between shZEB1/231^{K1108Q} and shZEB1/231^{K1108R} cells revealed that the former exhibited an epithelial-like state, while the latter adopted a classical mesenchymal phenotype (Fig. S5K). Notably, a significant increase in the number of upregulated differentially expressed genes (DEGs) was observed in shZEB1/231^{K1108Q} cells (Fig. 5H), demonstrating that acetylated ZEB1^{K1108} indeed switched from a classical transcriptional repressor to an activator. Through comparative analysis of these DEGs, we identified 51 key genes that were potentially modulated by the acetylation of ZEB1^{K1108} (Fig. 5I). Our investigation focused on genes that potentially maintain an epithelial-like state, including epithelial splicing regulatory protein (ESRP), junctional adhesion molecule 1 (JAM-1/F11R) and embigin (EMB) [21,22] (Fig. 5J), and revealed transcriptional activation of these epithelial-related genes by qPCR (Fig. 5K) and dual-luciferase reporter assays (Fig. 5L). Similar results were also observed in SUM-159 cells (Fig. S5L and S5M).

Since the K1108 site is located in the C-terminal region of ZEB1, we postulated that its acetylation might alter the interaction of ZEB1 with its transcriptional cofactors. Co-IP analysis revealed that ZEB1^{K1108R} was associated mainly with the corepressor CtBP, whereas ZEB1^{K1108Q} predominantly interacted with the transcriptional coactivator CBP (Fig. 5M). Experiments with SUM-159 cells yielded the similar results (Fig. S5N). We also verified these observations in tumour samples from the MMTV-PyMT and 4T1 orthotopic mouse models and found that Zeb1 was predominantly bound to Ctbp in the primary tumours; however, in the metastatic lung tumour samples, it preferentially interacted with Cbp (Fig. 5N). These findings were further confirmed by sequential ChIP analysis, which revealed significantly increased recruitment ZEB1 and CBP on the promoters of epithelial-related genes, such as E-cadherin, ESRP1, F11, and EMB, in shZEB1/231^{K1108Q} cells (Fig. 5O). Taken together, these results indicated that ZEB1^{K1108} acetylation specifically switches its cofactor-binding preference and subsequent transcriptional regulation mode, which leads to a hybrid epithelial-mesenchymal phenotype of TNBC cells with metastatic potential.

2.6. Acetylated ZEB1^{K1108} allows tumour cells to adapt to oxidative stress

Previous studies have demonstrated that cancer cell metastasis is linked to environmental oxidative stress, such as ROS production, which increases both the protein stability and catalytic activity of CBP [23,24]. Therefore, we treated MDA-MB-231 cells with H_2O_2 to simulate an oxidative stress environment. The results indicated that the protein level of endogenous CBP rose significantl in a dose- and time-dependent manner in response to H_2O_2 in both MDA-MB-231 (Fig. S6A) and SUM-159 cells (Fig. S6B). To further evaluate the effect of ROS on CBP, we employed a chemogenetic system in which D-amino acid oxidase (DAAO) was expressed to specifically generate H2O2 in response to D-Alanine(D-Ala). Consistent with previous reports [25,26], only D-Ala, but not L-alanine(L-ala), induced a significant increase in ROS production, as measured by DCFH/DA assay (Fig. S6C and S6D). Moreover, D-Ala treatment significantly increased the protein level of endogenous CBP in a dose-dependent manner (Fig. S6E and S6F). Additionally, either H_2O_2 (Fig. 6A) or D-Ala (Fig. 6B) treatment increased the self-acetylation of CBP at the K1535 site, which correlated with a significant increase in ZEB1^{K1108} acetylation. We also observed similar effects when another stimulus, sodium arsenite (SA), was used, confirming the increased ZEB1^{K1108} acetylation levels in response to oxidative stress (Fig. 6C). However, the addition of catalase, which breaks down H_2O_2, markedly attenuated ZEB1^{K1108} acetylation in MDA-MB-231 cells (Fig. 6D). We also performed these experiments in SUM-159 cells and obtained the same results (Fig. S6G–6J), which suggested that ZEB1^{K1108} acetylation was a potent effector of oxidative stress in TNBC cells.

To further investigate the ability of acetylated ZEB1^{K1108} to help cells cope with oxidative stress, we treated shZEB1/231^{WT} and shZEB1/231^{K1108R} cells with H_2O_2, respectively. Our observations revealed that compared with shZEB1/231^{WT} cells, shZEB1/231^{K1108R} cells presented significantly pronounced morphological changes, such as severe crumpling, enlarged and rounded shapes, and impaired cell edges (Fig. 6E). We also performed colony formation (Fig. 6F) and cell viability (Fig. 6G) assays, which revealed that the sensitivity of shZEB1/231^{K1108R} cells in response to H_2O_2-induced oxidative damage strongly increased. Similar effects were further obtained in SUM-159 cells (Fig. S6K–6M). Of note, consistent findings were validated in the D-Ala–induced H_2O_2 system (Fig. S6N–6Q) as well as in the oxidative stress models induced by either SA or t-BHP (Fig. S6R). Additionally, GSEA revealed upregulation of the gene set associated with ROS pathway in shZEB1/231^{K1108Q} cells

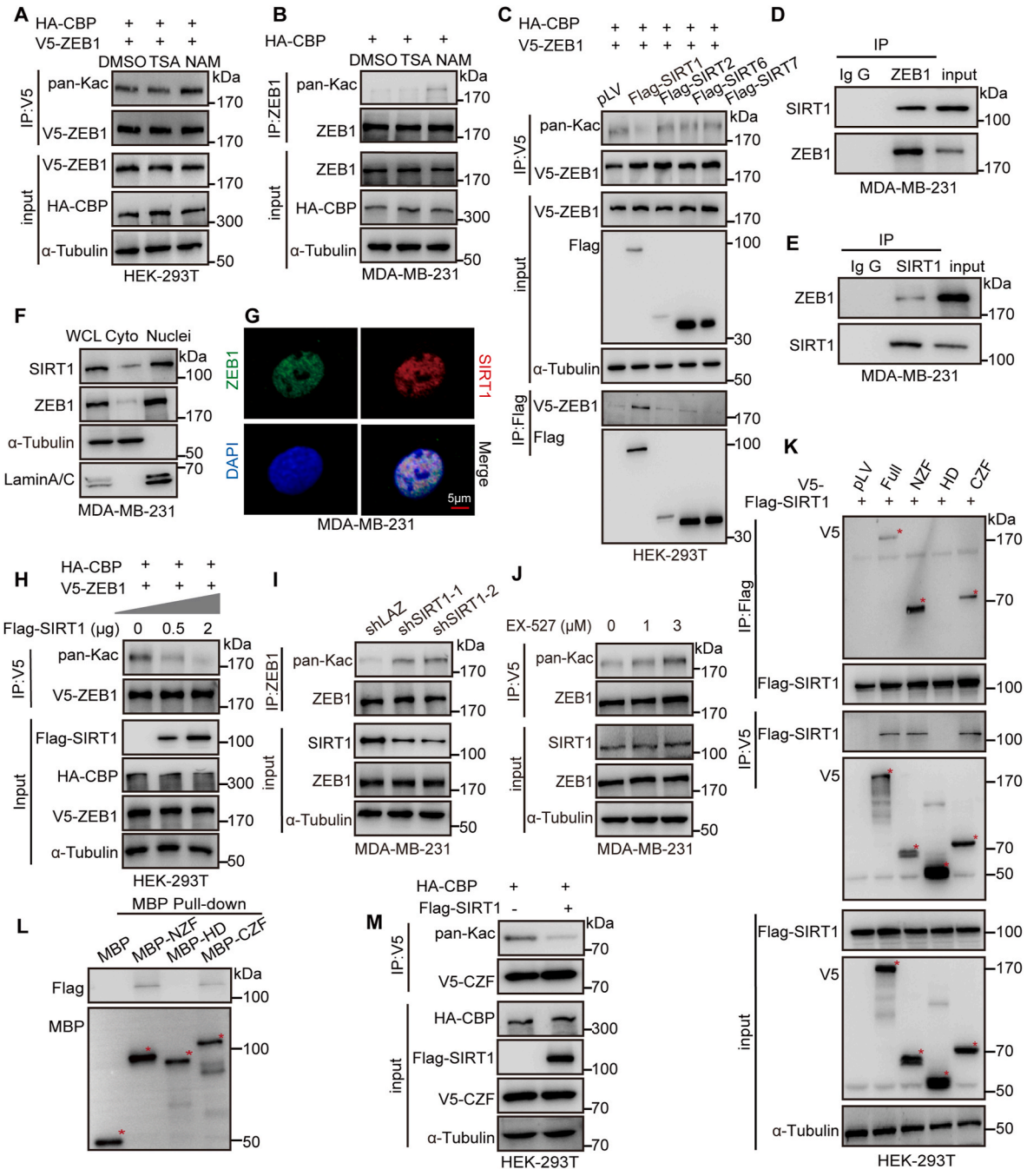

Fig. 3. SIRT1 specifically deacetylates ZEB1. (A, B) IB analysis with an anti-pan-Kac antibody in HEK-293T cells co-transfected with V5-ZEB1 and HA-CBP (A) and MDA-MB-231 cells transfected with HA-CBP for 48 h (B), followed by treatment with 2 μM TSA or 5 mM NAM for 12 h. **(C)** IP analysis with an anti-pan-Kac antibody in HEK-293T cells transfected with the indicated Flag-tagged SIRT family. **(D, E)** Co-IP analysis of endogenous ZEB1 and SIRT1 in MDA-MB-231 cells. **(F)** IB analysis of ZEB1 and SIRT1 in the WCL, cytosolic, and nuclear fractions of MDA-MB-231 cells. **(G)** Representative IF images of MDA-MB-231 cells stained with anti-ZEB1 and anti-SIRT1 antibodies. Scale bars: 5 μm. **(H)** IB analysis with an anti-pan-Kac antibody in HEK-293T cells co-transfected with V5-ZEB1, HA-CBP, and different doses of Flag-SIRT1. **(I)** IB analysis with an anti-pan-Kac antibody in MDA-MB-231 cells with SIRT1 knockdown. **(J)** IB analysis with an anti-pan-Kac antibody in MDA-MB-231 cells by treatment with different concentrations of EX-527 for 8 h. **(K)** Co-IP analysis in HEK-293T cells co-transfected with V5-tagged ZEB1 truncation mutants and Flag-SIRT1. **(L)** MBP pulldown assays in HEK-293T cells transfected with Flag-SIRT1. **(M)** IB analysis with an anti-pan-Kac antibody in HEK-293T cells co-transfected with V5-CZF and HA-CBP in the presence or absence of Flag-SIRT1.

compared with that in shZEB1/231^{K1108R} cells (Fig. 6H), highlighting that altered sulfur-based metabolism, increased NADPH production and increased activity of antioxidant transcription factors might be involved in ZEB1^{K1108} acetylation-triggered cell adaptation to oxidative stress [27]. Indeed, we observed significantly increased expression of various key enzymes involved in NADPH production, including *ME1*, *ME2*, and *G6PDH*, in shZEB1/231^{K1108Q} cells (Fig. 6I). Moreover, oxidative stress induced more pronounced decreases in GSH/GSSG and NADPH/NADP$^+$ ratios in shZEB1/231^{K1108R} cells than those in shZEB1/231^{K1108Q} cells, indicating that the loss of ZEB1^{K1108} acetylation impaired antioxidant defence mechanism and redox balance (Fig. 6J and K). We also performed these experiments in SUM-159 cells and obtained the same results (Fig. S7A–7C).

During metastasis, ferroptosis has been demonstrated to play a

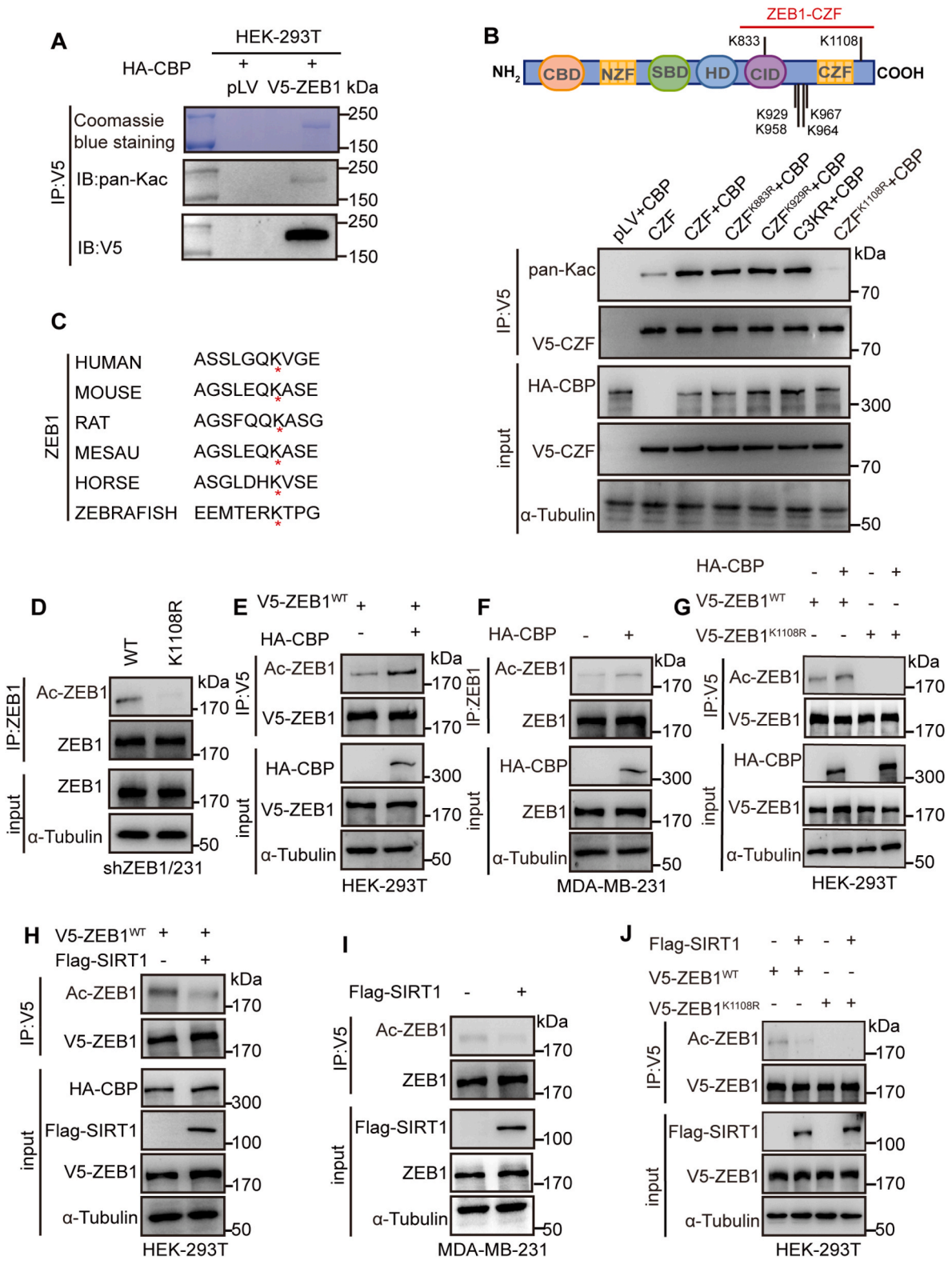

Fig. 4. K1108 is a critical acetylation site for ZEB1. (A) Identification of the acetylation site for ZEB1. HEK-293T cells were transfected with V5-ZEB1 and HA-CBP for 48 h, followed by treatment with 5 mM NAM for 12 h. **(B)** The indicated acetylated sites in CZF of ZEB1 were identified via MS (top panel). IB analysis was performed with an anti-pan-Kac antibody in HEK-293T cells co-transfected with V5-CZF mutants and HA-CBP (bottom panel). **(C)** Highly conserved amino acid of ZEB1^{K1108} across species. **(D)** IB analysis with an Ac-ZEB1 antibody in shZEB1/231^{WT} and shZEB1/231^{K1108R} cells. **(E)** IB analysis with Ac-ZEB1 antibody in HEK-293T cells co-transfected with V5-ZEB1^{WT} in the presence or absence of HA-CBP. **(F)** IB analysis with an Ac-ZEB1 antibody in MDA-MB-231 cells transfected with HA-CBP. **(G)** IB analysis with Ac-ZEB1 antibody in HEK-293T cells co-transfected with V5-ZEB1^{WT} or V5-ZEB1^{K1108R} in the presence or absence of HA-CBP. **(H)** IB analysis with Ac-ZEB1 antibody in HEK-293T cells co-transfected with V5-ZEB1^{WT} in the presence or absence of Flag-SIRT1. **(I)** IB analysis with an Ac-ZEB1 antibody in MDA-MB-231 cells transfected with Flag-SIRT1. **(J)** IB analysis with Ac-ZEB1 antibody in HEK-293T cells co-transfected with V5-ZEB1^{WT} or V5-ZEB1^{K1108R} in the presence or absence of Flag-SIRT1.

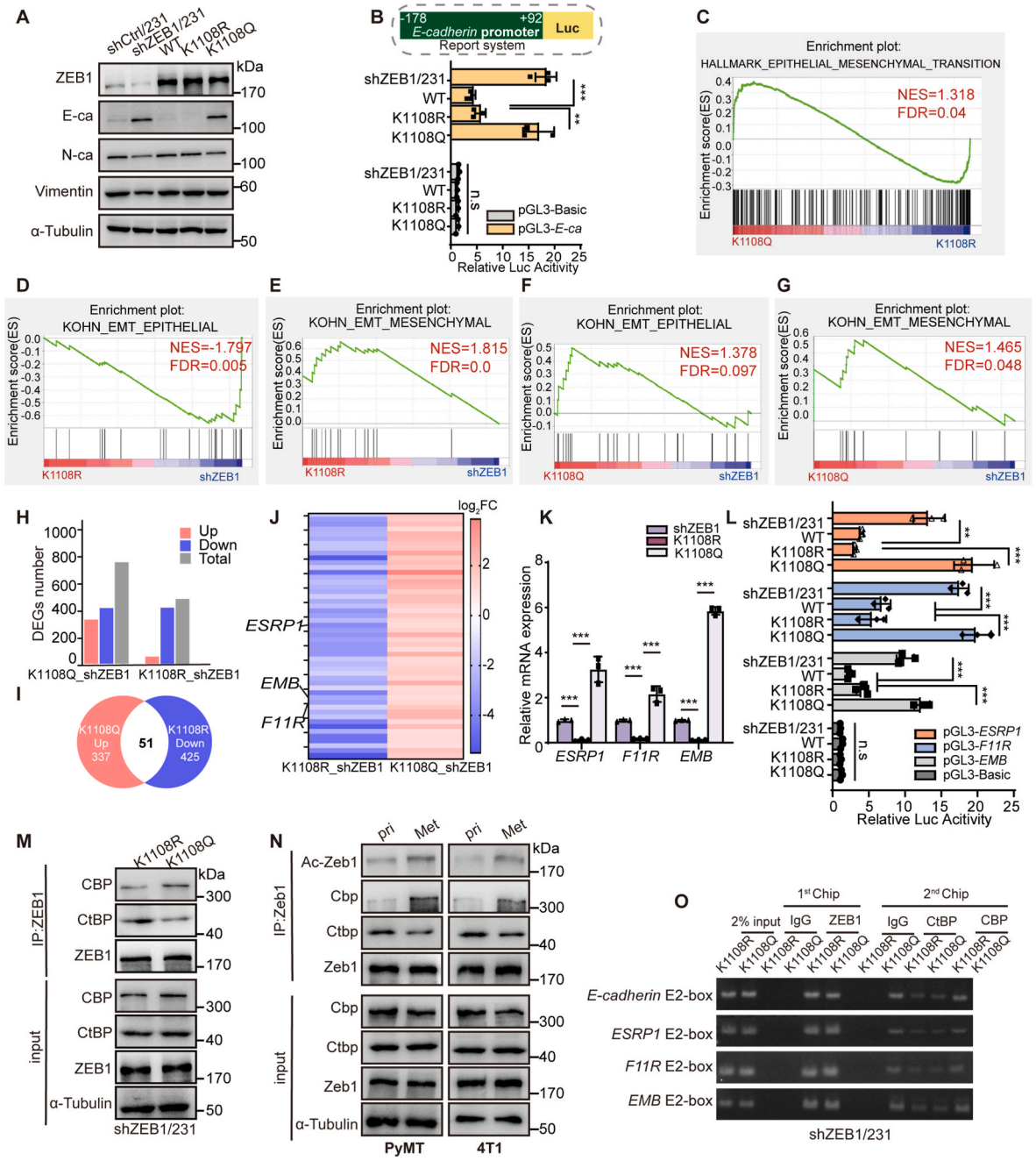

Fig. 5. Acetylation of ZEB1^{K1108} switches the transcriptional regulation mode of ZEB1. **(A)** IB analysis with epithelial- and mesenchymal-related gene antibodies in shCtrl/231, shZEB1/231, shZEB1/231^{WT}, shZEB1/231^{K1108R}, and shZEB1/231^{K1108Q} cells. **(B)** Dual luciferase assay for the *E-cadherin* promoter (−178/+92) in the indicated cells. **(C)** GSEA enrichment analysis of shZEB1/231^{K1108R} *vs.* shZEB1/231^{K1108Q} cells. NES, normalized enrichment score; FDR, false discovery rate. **(D–G)** GSEA enrichment analysis of shZEB1/231, shZEB1/231^{K1108R}, and shZEB1/231^{K1108Q} cells. **(H)** Statistical count of upregulated and downregulated DEGs ($P < 0.05$, FC > 1). **(I, J)** Venn diagram (I) and heatmap (J) of DEGs upregulated in shZEB1/231^{K1108Q} cells and downregulated in shZEB1/231^{K1108R} cells. **(K)** Relative mRNA levels of *ESRP1*, *F11*, and *EMB* in the indicated cells. **(L)** Dual luciferase assays for the *ESRP1*, *F11*, and *EMB* promoters in the indicated cells. **(M)** Co-IP analysis of ZEB1, CBP, and CtBP in shZEB1/231^{K1108R} and shZEB1/231^{K1108Q} cells. **(N)** Co-IP analysis of Zeb1, Cbp, and Ctbp in primary tumours and lung metastases from PyMT and 4T1 orthotopic metastasis models. **(O)** Sequential ChIP analysis of the co-occupation of E_2-box elements in the *E-Cadherin* (−23), *ESRP1* (-100), *F11* (−124), and *EMB* (−190) promoters by association of ZEB1 with CBP or CtBP in shZEB1/231^{K1108R} and shZEB1/231^{K1108Q} cells. According to the two-tailed Student's *t*-test, the error bars represent the means ± SDs, n = 3.

pivotal role in enabling cancer cells to adapt to oxidative stress, which is characterized by iron overload, ROS accumulation, and lipid peroxidation [28]. As shown in Fig. 6L, the level of GPX4 was markedly reduced in shZEB1/231^{K1108R} cells, whereas that of ACSL4 was significantly increased, indicating that shZEB1/231^{K1108R} cells underwent more severe ferroptosis than shZEB1/231^{WT} cells did. BODIPY C11 staining and transmission electron microscopy further confirmed the increased lipid peroxidation levels in shZEB1/231^{K1108R} cells (Fig. 6 M – 6O). The same results were also observed in SUM-159 cells (Fig. S7D and S7E). Importantly, we conducted a dynamic competition experiment between CBP and CtBP in shZEB1/231^{WT} and shZEB1/231^{K1108R} cells. Under oxidative stress, cofactor interactions were altered in shZEB1/231^{WT} cells, in which the acetylation of ZEB1^{K1108} disrupted its interaction with CtBP and promoted that with CBP, whereas shZEB1/231^{K1108R} cells

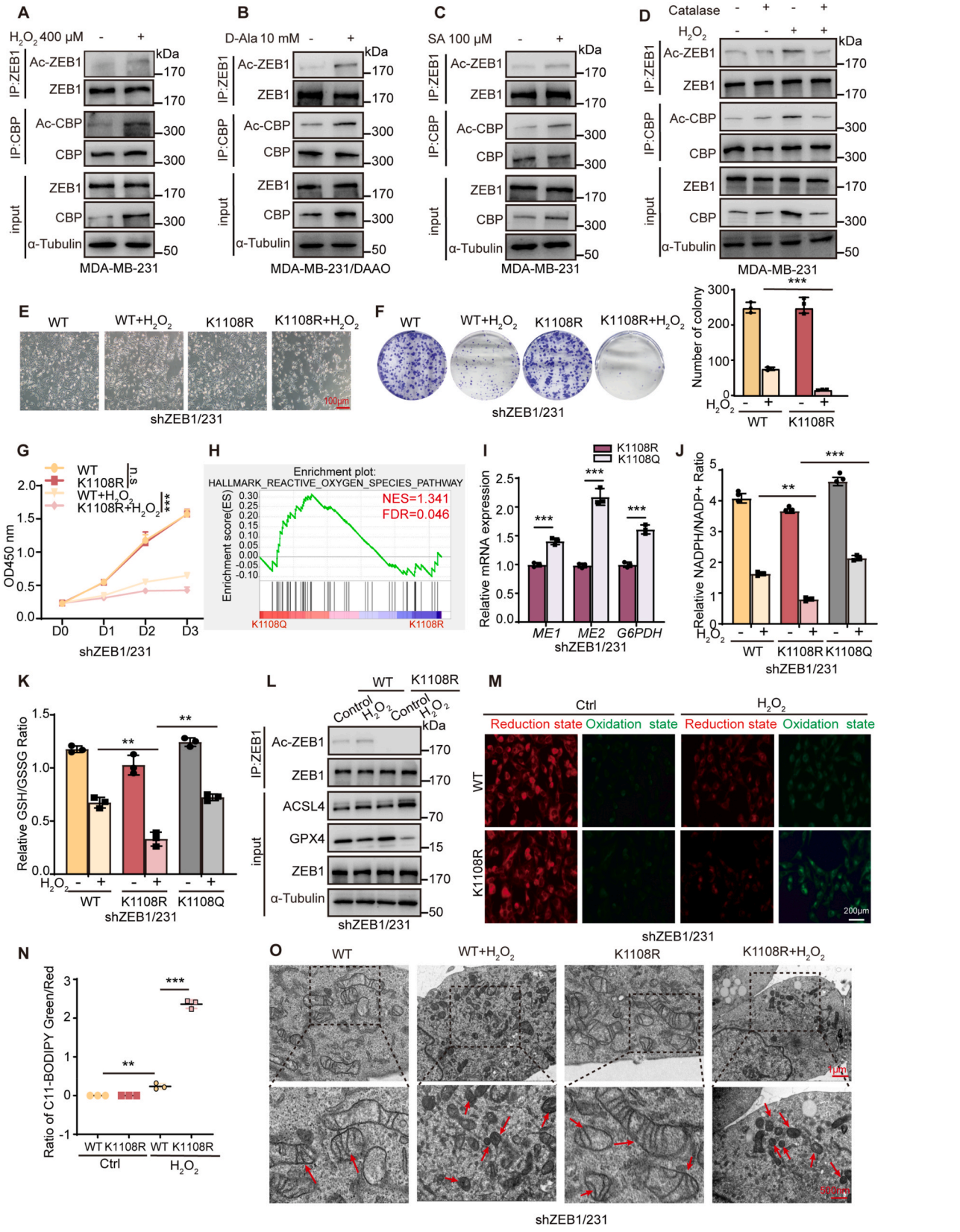

(caption on next page)

Fig. 6. Acetylated ZEB1^{K1108} allows tumour cells to adapt to oxidative stress. (A) IB analysis with Ac-ZEB1 antibody in MDA-MB-231 cells by treatment with 400 μM H_2O_2 for 3 h. **(B)** IB analysis with Ac-ZEB1 antibody in MDA-MB-231/DAAO cells by treatment with 10 mM D-Ala for 6 h. **(C)** IB analysis with Ac-ZEB1 antibody in MDA-MB-231 cells by treatment with 100 μM sodium arsenite for 3 h. **(D)** IB analysis with Ac-ZEB1 antibody in MDA-MB-231 cells treated with 400 μM H_2O_2 for 3 h, followed by treatment with catalase for 1.5 h. **(E)** Representative phase contrast images of MDA-MB-231 cells treated with 400 μM H_2O_2 for 3 h. **(F, G)** Analysis of colony formation (F) and cell viability (G) in shZEB1/231^{WT} and shZEB1/231^{K1108R} cells by treatment with 150 μM H_2O_2. **(H)** GSEA enrichment analysis of transcriptome data from shZEB1/231^{K1108Q} cells *vs.* shZEB1/231^{K1108R} cells. **(I)** Relative mRNA levels of *ME1*, *ME2,* and *G6PDH* in shZEB1/231^{K1108R} and shZEB1/231^{K1108Q} cells. **(J)** Relative NADPH/$NADP^+$ ratio in shZEB1/231^{WT}, shZEB1/231^{K1108R}, and shZEB1/231^{K1108Q} cells by treatment with 400 μM H_2O_2 for 3 h. **(K)** Relative GSH/GSSG ratio in shZEB1/231^{WT}, shZEB1/231^{K1108R}, and shZEB1/231^{K1108Q} cells by treatment with 400 μM H_2O_2 for 3 h. **(L)** IB analysis with Ac-ZEB1, ACSL4, and GPX4 in shZEB1/231^{WT} and shZEB1/231^{K1108R} cells by treatment with 400 μM H_2O_2 for 3 h. **(M, N)** Representative BODIPY™ 581/591 C11 staining images of shZEB1/231^{WT} and shZEB1/231^{K1108R} cells by treatment with 400 μM H_2O_2 for 3 h. **(O)** Representative transmission electron microscopy images of mitochondrial ferroptosis in shZEB1/231^{WT} and shZEB1/231^{K1108R} cells by treatment with 400 μM H_2O_2 for 3 h. The red arrow indicates mitochondria. According to the two-tailed Student's *t*-test, the error bars represent the means ± SDs, n = 3.

failed to respond (Fig. S7F). In conjunction with previous findings showing that mesenchymal-like cancer cells are more sensitive to ferroptosis-related oxidative damage [29], we proposed that acetylated ZEB1^{K1108} contributes to a hybrid epithelial-mesenchymal phenotype of TNBC cells, thereby increasing their antioxidant capacity during metastasis.

2.7. *ZEB1^{K1108} acetylation promotes breast cancer lung metastasis in vivo*

To further test the effects of ZEB1 acetylation on breast cancer development and metastasis *in vivo*, we used a 4T1 cell orthotopic metastasis model. As shown in Fig. 7A, shZeb1/4T1 cells stably expressing Zeb1^{WT} and Zeb1^{K1094R} were injected into the fourth mammary fat pad of female BALB/c mice, the primary tumours were surgically excised after 12 days, and the lung tissues were harvested after 60 days. We found that Zeb1^{K1094} acetylation did not affect the volume of primary tumours (Fig. 7A and B). However, compared with those of control tumours from wild-type Zeb1 orthotopic mice, lung metastases were significantly reduced in Zeb1^{K1094R} tumour-bearing mice (Fig. 7C), as indicated by decreases in number of metastatic foci (Fig. 7D), the metastatic foci area occupying the total lung area (Fig. 7E), and the lung weight (Fig. 7F). We also found that the expression levels of Zeb1 were comparable in both primary tumours and lung metastatic foci from wild-type Zeb1-and Zeb1^{K1094R}-expressing tumours. However, the acetylation level of Zeb1^{K1094} was significantly increased in lung metastases from wild-type Zeb1-expressing tumour (Fig. 7G). As expected, the acetylation of Zeb1^{K1094} was not detected in either primary or metastatic Zeb1^{K1094R}-expressing tumours. Notably, IF staining confirmed that lung metastases presented a hybrid epithelial-mesenchymal phenotype, with relatively high E-cadherin expression in wild-type Zeb1-expressing tumours (Fig. 7H). Together, our observations confirmed that Zeb1 acetylation leads to a hybrid epithelial-mesenchymal phenotype to promote lung metastasis of TNBC *in vivo*.

3. Discussion

During breast cancer lung metastasis, EMP is crucial for tumour cells to adapt to microenvironmental stresses [30]. Our study revealed that oxidative stress increased ZEB1 acetylation at the K1108 site, thereby inducing a hybrid epithelial-mesenchymal phenotype. This modification improved cell survival by promoting resistance to oxidative damage, preventing ferroptosis, and facilitating lung metastasis.

Recent studies have shown that ZEB1, a classical transcriptional repressor, can also exert transactivation effects in synergy with co-transcriptional activators [31]. For example, Li et al. demonstrated that ZEB1, in complex with the coactivator p300, was enriched in the DNMT1 promoter, thereby promoting its transcriptional activation and increasing lung metastasis in breast cancer [32]. In addition, ZEB1 can be indirectly recruited to DNA through interaction with factors, such as Lef1, AP-1 and YAP, which further facilitate its role in transcriptional activation [33–35]. However, the mechanism of dynamic transition between transcriptional repression and activation by ZEB1 under microenvironmental stress remains to be elucidated. In the present study, we provided further evidence that oxidative stress could increase the acetylation of ZEB1^{K1108} during metastatic colonization of the lung by TNBC cells, thus altering its ability to interact with different co-transcriptional factors. This finding is consistent with previous study showing that ZEB1 acetylation disrupts its interaction with the transcriptional repressor CtBP [36]. Notably, our results also demonstrated that under oxidative stress, activation of CBP led to a significant increase in ZEB1^{K1108} acetylation, thereby increasing the expression of adhesion- and epithelial-related genes, such as E-cadherin. Given that ZEB1^{K1108} is located adjacent to the CtBP interaction domain (CID) and has a strong binding affinity for CtBP, we speculated that ZEB1 acetylation at K1108 might alter the conformation of its carboxyl terminus and lead to alternations in co-transcriptional factors that bind to ZEB1.

Consistently, oxidative stress, such as high levels of ROS, poses a significant challenge to the survival of tumour cells that metastasize through the circulation [37]. During this process, acetylation can rapidly adapt protein function to counteract the effects of ROS. For example, ROS can increase the self-acetylation of several acetylases, such as CBP [23] and p300 [38], while also regulating the deacetylation capacities of members of the SIRT family by modulating the NADPH/-NADH ratio [39]. Additionally, in both the PyMT and 4T1 orthotopic tumor metastasis models, we observed significantly reduced SIRT1 enzymatic activity in lung metastatic lesions compared to primary tumours (data not shown). Based on previous reports demonstrating that CBP acetylates SIRT1 and inhibits its deacetylase activity [40], we propose that the accumulation of ZEB1^{K1108} acetylation in the lung metastasis results from enhanced CBP-mediated acetylation and impaired SIRT1-dependent deacetylation. However, further studies are needed to elucidate the detailed mechanisms. Furthermore, ROS levels are critical for the reversible transition of cancer stem cells (CSCs) between epithelial and mesenchymal states. Low ROS levels maintain CSCs in a quiescent mesenchymal state, whereas elevated ROS levels promote their transition to a proliferative epithelial state [27,41]. In line with these findings, our study revealed that ROS could modify ZEB1 activity through acetylation modification, thus creating a hybrid epithelial-mesenchymal phenotype of TNBC cells with high metastatic potential to the lung.

Phenotypic plasticity allows tumour cells to dynamically change in response to various stresses encountered during malignant progression, which is a key mechanism that promotes metastasis, treatment resistance and metabolic dysfunction. Among these adaptations, ZEB1-induced cellular plasticity enables tumour cells to overcome environmental stress by switching between different phenotypes. Studies have shown that alterations in ZEB1 chromatin accessibility significantly influence cellular plasticity in various human cancers. For example, Chaffer et al. reported that the bivalent chromatin configuration of ZEB1 promoter responds to signals from the inflammatory microenvironment, thereby causing breast cancer cells to frequently switch between low and high tumourigenic states [42]. Wang et al. also showed that ZEB1-driven metabolic reprogramming allowed prostate cancer cells to undergo epigenetic reprogramming, which further facilitates the switch from a glandular lineage to a neuroendocrine lineage [43]. Taken together, our results suggested that triggering EMP

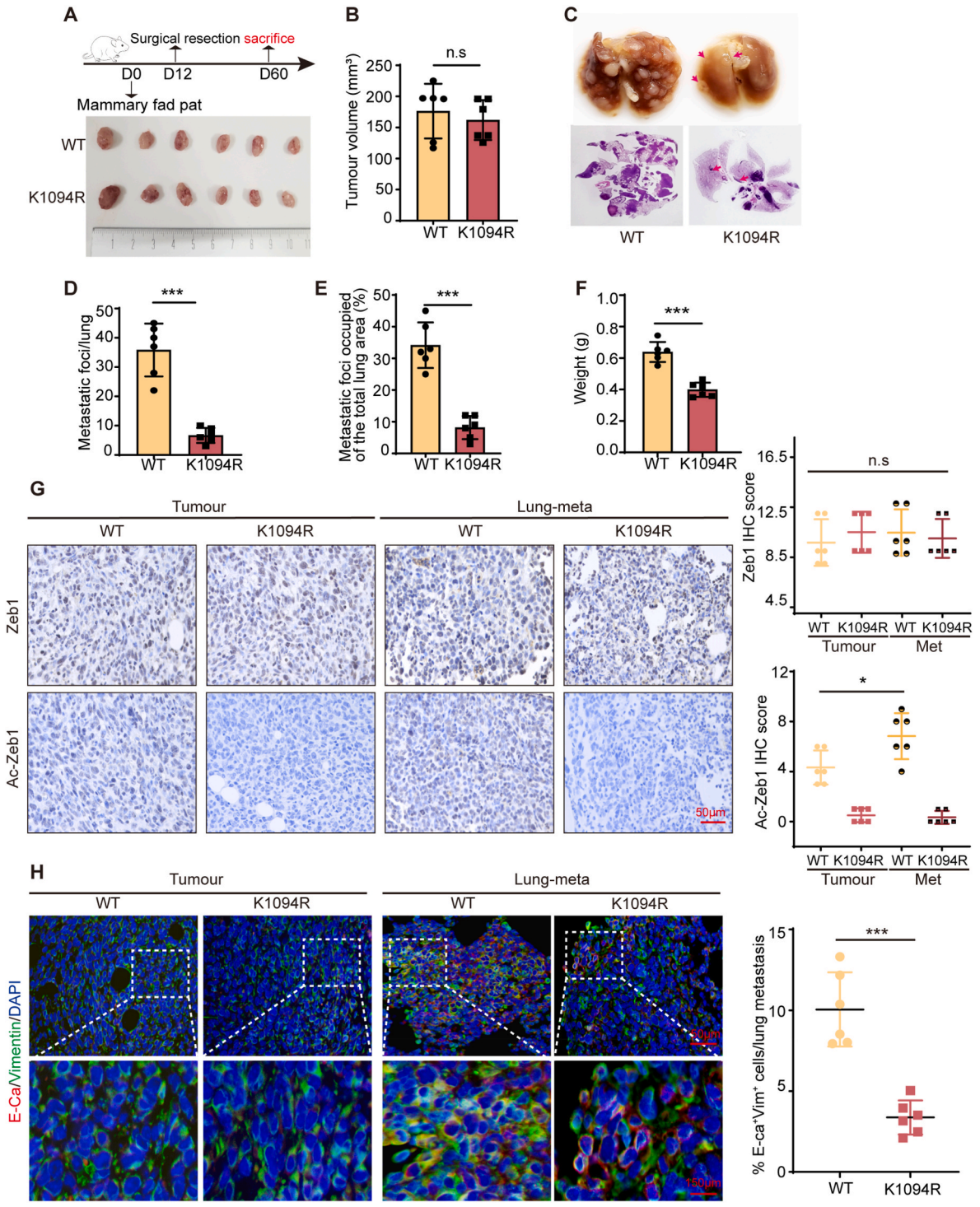

Fig. 7. ZEB1^{K1108} acetylation promotes breast cancer lung metastasis *in vivo*. **(A)** Schematic of the 4T1 orthotopic metastasis model (top panel) with shZeb1/4T1^{WT} and shZeb1/4T1^{K1094R} cells. The lower panel shows tumours derived from shZeb1/4T1^{WT} and shZeb1/4T1^{K1094R}-bearing mice. **(B)** The approximate volume of tumours from the indicated tumour-bearing mice. **(C)** Representative images and HE-stained sections of metastatic lung nodules from the indicated tumour-bearing mice. **(D–F)** The approximate number of metastatic foci (D), the metastatic foci area occupying the total lung area (E), and the lung weight (F) in the indicated tumour-bearing mice. **(G)** Representative images of IHC staining using Ac-Zeb1 and Zeb1 antibodies in primary tumours and lung metastases. **(H)** Representative IF images of E-cadherin and Vimentin in primary tumours and lung metastases. Two-tailed Student's *t*-test was used. The error bars represent the means ± SDs, n = 6.

by ZEB1 might be a critical mechanism through which tumour cells respond to environmental stress factors, such as ROS. Additionally, cancer cells in the mesenchymal state are generally resistant to apoptosis that is induced by conventional therapies but are sensitive to ferroptosis, which might be associated with high ZEB1 expression [44]. Consistently, research by Schwab et al. also showed that, in mesenchymal tumour cells, ZEB1 upregulates the expression of polyunsaturated fatty acid-related genes, thus increasing the sensitivity of these cells to ferroptosis [29]. In the present study, by using an oxidative stress-induced ferroptosis model, we observed that TNBC cells with the ZEB1^{K1108R} mutation presented classical mesenchymal cell sensitivity to ferroptosis. In contrast, cells with the wild-type ZEB1 exhibited a hybrid

epithelial-mesenchymal phenotype, allowing a small subset of cells to survive under oxidative stress. Although the specific mechanism by which acetylated ZEB1 reduces the sensitivity to ferroptosis remains unclear, our findings highlighted hybrid epithelial-mesenchymal plasticity as a critical adaptive strategy for tumour cell survival under oxidative stress. Our study thus extended the understanding of mechanism involved by exploring PTMs, specifically mediated by ZEB1 acetylation, as a critical apparatus that enables tumour cells to respond more precisely to microenvironmental cues, which eventually affect EMP.

Collectively, our mechanistic study demonstrated that ZEB1 was dynamically acetylated and deacetylated at K1108 by CBP and SIRT1, respectively. This acetylation weakened the binding of ZEB1 to CtBP and altered its transcriptional regulation mode, ultimately inducing a hybrid epithelial-mesenchymal state of TNBC cells. Our research also elucidated the specific mechanisms of ZEB1 acetylation in TNBC cell survival and metastasis under oxidative stress. These findings provided a theoretical foundation for understanding how ZEB1 acetylation influences EMP and antioxidant responses, opening new avenues for developing novel treatment strategies for advanced breast cancer.

4. Material and methods

4.1. Cell culture and plasmids

The breast cancer cell lines MDA-MB-231, SUM-159, 4T1, and HEK-293T were acquired from the American Type Culture Collection (Manassas, VA, USA). MDA-MB-231 cells were grown in RPMI-1640 medium, and SUM-159, 4T1, and HEK-293T cells were cultured in DMEM supplemented with 10 % foetal bovine serum and 100 U/ml pen/strep. All the cells were maintained in a Thermo humidified incubator with 5 % CO_2. All of the reagents listed above were supplied by Biological Industries (Israel).

The human cDNA fragments of acetyltransferases (PCAF, HMOF, and TIP60), deacetylases (SIRT1, SIRT2, SIRT6, and SIRT7), and ZEB1 were subcloned and inserted into pLV-EF1-MCS-IRES-Bsd (Biosettia) as entry clones expressing C-tagged fusion proteins. All the deletion and point mutants were generated via PCR and verified by sequencing (Sangon). The sequences of the primers are listed in Supplementary Table 3. The shRNA target sites were selected via Thermo Fisher RNAi Designer (http://rnaidesigner.thermofisher.com/rnaiexpress/), and the shRNA templates were inserted into the lentiviral-based vector pLV-H1-EF1α-puro (Biosettia), which was used for the expression of shRNAs. The human *E-cadherin*, *ESRP1*, *EMB,* and *F11* promoters were subsequently cloned and inserted into the pGL3 basic vector (Promega). HA-CBP and HA-p300 were kindly provided by Dr. Hongquan Zhang.

4.2. Antibodies and reagents

The Ac-ZEB1 polyclonal antibody was produced and purified with ABclonal. A rabbit polyclonal antibody specific for acetylated lysine K1108 of ZEB1 (Ac-ZEB1) was generated via the synthetic peptide SSLGQK(ac)VGESSE.

The following specific antibodies were used: ZEB1 (Proteintech, 21544-1-AP for WB and IP; Santa Cruz, sc-515797 for IP and Chip; Servicebio, GB11513 for IHC), anti-acetylated lysine (Cell Signalling, 9441), CBP (PTM-bio, PTM-5281), CBP-1535Ac (Cell Signalling, 4771), SIRT1 (Proteintech, 60303-1-Ig), V5 (Cell Signalling, 13202 for WB; Proteintech, v5tma for IP; Thermo, R960-25 for WB and IP), HA (Cell Signalling, 3724 for WB; AlpaLifebio, KTSM1005 for IP), Flag (Cell Signalling, 1382 for WB; AlpaLifebio, KTAN1008 for IP), GPX4 (SAB, 49731), ACSL4 (Santa Cruz, sc-365230), E-cadherin (BD, 610182 for WB; Servicebio, GB12083 for IHC), vimentin (Cell Signalling, 5741), N-cadherin (Cell Signalling, 1494), α-tubulin (Proteintech, 66031-1-Ig), and LaminA/C (Proteintech, 10298-1-Ig). A485 (MCE, HY-107455), a selective catalytic inhibitor of p300/CBP, was used at a final concentration of 3 μM. TSA (TargetMol, T6270) and nicotinamide (MCE, HY-B0150) were used at final concentrations of 1 μM and -5 mM, respectively. EX-527 (MCE, HY-15452), a potent and selective SIRT1 inhibitor, was used at a final concentration of 1 μM. NAC (TargetMol, T0875) was used at 1 mM, and sodium arsenite (Aladdin, S463149) was used at 100 μM.

4.3. RNA extraction and quantitative RT-PCR

Total RNA was extracted from the samples via the TRIeasy™ Total RNA Extraction Reagent (Yeasen, 10606ES60). Reverse transcription was carried out via a first-strand cDNA synthesis Hifair® II 1st Strand cDNA Synthesis Kit (Yeasen, 119119ES60). Specifically, the products were amplified via quantitative PCR via Hieff UNICON® qPCR SYBR Green Master Mix (Yeasen, 11200ES08). GAPDH was used as a normalization control. Three replicates were set for each sample, and the sequences of the primers are listed in Table S3.

4.4. Immunoblotting

The cells were lysed with RIPA buffer (Yeasen, 20115ES60) supplemented with protease inhibitors (Yeasen, 20123ES10), PMSF (Beyotime, ST506), and HDACi (Beyotime, P1112). The samples were vortexed for 1 min and then lysed on ice for 20 min, followed by sonication on ice for 2 min. The supernatant was collected after high-speed centrifugation (12000 g, 4 °C), and the protein concentration was determined via BCA (Yeasen, 20201ES76). The standard Western blotting procedures included electrophoresis, membrane transfer, blocking with 5 % milk, and antibody incubation for analysis.

4.5. Immunoprecipitation (IP) assay

A total of 350 μg (exogenous proteins extracted from HEK-293T cells) or 1 mg (protein extracted from breast cancer cells) of total protein was incubated with agarose beads or Ab-coated magnetic beads overnight with rotation. The precipitated proteins were eluted with 2 × SDS sample buffer for 10 min at 100 °C and analysed via WB.

4.6. IP-MS for identifying the acetylation site of ZEB1

Cell extracts from V5-ZEB1-transfected HEK-293T cells were subjected to IP via V5-coated magnetic beads, separated via SDS-PAGE and stained with Coomassie Brilliant Blue. After staining, the bands were excised and subjected to in-gel tryptic digestion. Peptides were analysed by tandem mass spectrometry (MS/MS) using an NSI source coupled online with UPLC on a Q ExactiveTM Plus (Thermo). The MS/MS data generated were processed via Proteome Discoverer 1.3, where tandem mass spectra were searched against the ZEB1 database. High confidence settings were used for peptide identification, and the peptide ion score threshold was set to >20.

4.7. MBP pulldown assay

MBP-labelled proteins were purified from DH5α (singke, TSC-C14) and incubated with amylose resin beads for 2–4 h with rotation. HA-CBP and Flag-SIRT1 were expressed in HEK-293T cells via plasmid transfection. The prepared amylose resin beads were then mixed with 1 mg of total cell lysate, and the mixture was incubated overnight at 4 °C on an end-over-end mixer. After three washes with cold PBS, the beads were boiled in 2 × SDS loading buffer and then subjected to Western blot analysis with the appropriate antibodies.

4.8. Orthotopic breast cancer mouse model

Female BALB/c mice (8 weeks old) were purchased from Hua Fukang (Beijing, China). Each mouse received an injection of 100 μL of PBS containing 1×10^4 4T1 cells into the fourth mammary fat pad. On day

12, the mice were anaesthetized (intraperitoneal, and the primary tumours were surgically removed). On day 60, the mice were euthanized, and their lungs were harvested to assess the number and size of pulmonary metastatic foci.

4.9. Immunohistochemical (IHC) staining

For IHC staining, tissue sections were deparaffinized with xylene and graded ethanol. Antigens were exposed by microwaving in citrate buffer for 30 min, followed by eliminating endogenous peroxidase activity with 0.3 % hydrogen peroxide solution for 10 min at room temperature. After blocking with 3 % BSA for 1 h, specific antibodies were applied to the sections. Colour development was performed via a DAB kit (Zsbio, ZLI-9018). The H-score method was used to assess the percentage of positively stained cells and the intensity of staining.

4.10. Immunofluorescence (IF) staining

For the IF assay, 2×10^4 MDA-MB-231 and SUM-159 cells were seeded on coverslips in 24-well plates. After attachment, the cells were washed with cold PBS, fixed with 4 % PFA and permeabilized with 0.1 % Triton X-100. The slides were then blocked with 5 % goat serum and incubated with primary antibodies overnight at 4 °C and secondary antibodies for 1 h at room temperature. After further washes, the nuclei were stained with DAPI (0.1 μg/ml, Beyotime, C1002). Images were captured via a fluorescence microscope (Olympus FV 1000) and analysed via ImageJ.

For tissue IF, tissue sections were deparaffinized and heated for antigen exposure as in IHC. After they cooled naturally, the sections were blocked with 5 % goat serum. The next steps were the same as those described above.

4.11. Dual luciferase assay

The cells were transfected with 1.5 μg of the indicated promoters in 24-well plates. At 48 h posttransfection, luciferase assays were performed via the Dual-Luciferase Reporter Assay System (Promega, E1910) according to the manufacturer's protocols. Luciferase activity was normalized to Renilla luciferase values. Three independent experiments were carried out with similar results.

4.12. Chromatin immunoprecipitation (ChIP)

ChIP assays were performed via the SimpleChIP® Enzymatic Chromatin IP Kit (CST, 9003). Briefly, the cells were crosslinked with 1 % formaldehyde for 10 min at room temperature, and the formaldehyde was then inactivated by the addition of 125 mM glycine. Chromatin was digested with micrococcal nuclease and sonicated to produce fragments. Chromatin extracts containing DNA fragments of 150–900 base pairs were immunoprecipitated with specific antibodies. The ChIP-enriched DNA was then uncrosslinked and analysed via PCR.

4.13. C11-BODIPY 581/591 staining

C11-BODIPY 581/591 (Sigma, SML3717) was used to measure lipid peroxidation. The cells were incubated with 1 mL of 3 μM BODIPY 581/591 C11 solution at 37 °C for 30 min, after which the dye was washed away. The levels of oxidation and reduction in the cells were captured via fluorescence microscopy, and the intensity of C11-BODIPY fluorescence was measured via ImageJ.

4.14. TEM

The cells were fixed in cacodylate-buffered 2.5 % (w/v) glutaraldehyde, postfixed in 2.0 % osmium tetroxide, and embedded in epoxy resin. The resin blocks were sectioned at 60–80 nm with an ultramicrotome, and the tissues were floated on 150 mesh cuprum grids with Formvar film. The slides were subjected to 2 % uranium acetate saturated alcohol solution to avoid light staining for 8 min, rinsed 3 times in 70 % ethanol and then rinsed 3 times in ultrapure water; 2.6 % lead citrate was used to avoid CO_2 staining for 8 min, after which they were rinsed 3 times with ultrapure water. After drying through the filter paper, the cuprum grids were placed on a grid board and dried overnight at room temperature. Images were scanned via a Hitachi HT7800/HT7700 microscope.

4.15. Colony formation assay

For the colony formation assays, 500–1000 cells were seeded in a 6-well plate. After attachment, the cells were treated with 150 μM H_2O_2 and incubated at 37 °C with 5 % CO_2 for 8–12 days. Colonies were fixed with 4 % PFA, stained with crystal violet, photographed and counted. A total of 3 independent experiments were carried out with similar results.

4.16. Chemogenetic activation of DAAO and ROS detection by DCFH-DA

Cells stably expressing DAAO were treated with 10 mM D-Alanine (Macklin, D800716) or L-alanine (Macklin, L800640) for 6 h. ROS levels were then assessed using a DCFH-DA assay kit (Beyotime, S0033S) according to the manufacturer's instructions. Fluorescence was detected at an excitation wavelength of 488 nm using a fluorescence microscope.

4.17. GSH/GSSG and NADPH/$NADP^+$ ratio measurement

Cells were incubated with 400 μM H_2O_2 for 3 h, cells were harvested and lysed in assay buffer. The GSH/GSSG and NADPH/$NADP^+$ ratios were measured using commercial assay kits (Beyotime, S0053 and Elabscience, E-BC-K803, respectively) according to the manufacturers' instructions. Absorbance was detected using a microplate reader.

4.18. Statistical analysis

All experimental data were analysed via GraphPad Prism 8 software and are presented as the means ± standard deviations (SDs). Two-tailed Student's *t* tests were used for pairwise comparisons. Each figure and statistical result were derived from at least three independent experiments to ensure reproducibility. Statistical significance levels are indicated as follows: * for $P < 0.05$, ** for $P < 0.01$ and *** for $P < 0.001$.

CRediT authorship contribution statement

Min Guo: Writing – review & editing, Writing – original draft, Methodology, Conceptualization. **Yan-Jing Wang:** Methodology. **Jie Shi:** Methodology. **Li-Xia Cao:** Methodology. **Yang Ou:** Methodology. **Xiao Jia:** Methodology. **Chun-Chun Qi:** Methodology. **Zhao-Xian Li:** Methodology. **Yu-Xin Liu:** Methodology. **Si-Yu Zuo:** Methodology. **Qiu-Ying Shuai:** Methodology. **Tian-Wen Yu:** Methodology. **Hua-Yu Hu:** Validation. **Xiao Chen:** Validation. **Meng-Dan Feng:** Methodology. **Yao Xue:** Validation. **Hang Wang:** Validation. **Pei-Qing Sun:** Validation. **Lei Liu:** Conceptualization. **Yi Shi:** Writing – review & editing, Conceptualization. **Shuang Yang:** Writing – review & editing, Funding acquisition, Conceptualization.

Ethical approval

This study adheres to the requirements approved by the Animal Ethics Committee of Nankai University under protocol number 2021-SYDWLL-000040, ensuring the maximization of animal welfare and strict compliance with relevant ethical guidelines.

Funding

This work was supported by grants from the International Science and Technology Cooperation Project of China (No. 2022YFE0133300) and National Natural Science Foundation of China (No. 82472870 and No. 82172801).

Declaration of competing interest

None declared.

Appendix A. Supplementary data

Supplementary data to this article can be found online at https://doi.org/10.1016/j.redox.2025.103834.

Data availability

Data will be made available on request.

References

[1] F. Bray, et al., Global cancer statistics 2022: GLOBOCAN estimates of incidence and mortality worldwide for 36 cancers in 185 countries, CA Cancer J. Clin. 74 (3) (2024) 229–263.
[2] S. Lin, et al., Clinicopathological characteristics and survival outcomes in patients with synchronous lung metastases upon initial metastatic breast cancer diagnosis in Han population, BMC Cancer 21 (1) (2021) 1330.
[3] A.W. Lambert, R.A. Weinberg, Linking EMT programmes to normal and neoplastic epithelial stem cells, Nat. Rev. Cancer 21 (5) (2021) 325–338.
[4] T.Y. Na, et al., The functional activity of E-cadherin controls tumor cell metastasis at multiple steps, Proc. Natl. Acad. Sci. U. S. A. 117 (11) (2020) 5931–5937.
[5] V. Padmanaban, et al., E-cadherin is required for metastasis in multiple models of breast cancer, Nature 573 (7774) (2019) 439–444.
[6] J. Cui, et al., MLL3 loss drives metastasis by promoting a hybrid epithelial-mesenchymal transition state, Nat. Cell Biol. 25 (1) (2023) 145–158.
[7] N. Aceto, et al., Circulating tumor cell clusters are oligoclonal precursors of breast cancer metastasis, Cell 158 (5) (2014) 1110–1122.
[8] C.N. Wong, et al., Identification and characterization of metastasis-initiating cells in ESCC in a multi-timepoint pulmonary metastasis mouse model, Adv. Sci. (Weinh.) 11 (30) (2024) e2401590.
[9] J. Lu, et al., ZEB1: catalyst of immune escape during tumor metastasis, Biomed. Pharmacother. 153 (2022) 113490.
[10] Y. Zhou, et al., ZEB1 enhances warburg effect to facilitate tumorigenesis and metastasis of HCC by transcriptionally activating PFKM, Theranostics 11 (12) (2021) 5926–5938.
[11] Z. Zhang, et al., CDK4/6 inhibition blocks cancer metastasis through a USP51-ZEB1-dependent deubiquitination mechanism, Signal Transduct. Targeted Ther. 5 (1) (2020) 25.
[12] M. Ouled Dhaou, et al., Zeb1 expression by tumor or stromal cells is associated with spatial distribution patterns of CD8+ tumor-infiltrating lymphocytes: a hypothesis-generating study on 113 triple negative breast cancers, Am. J. Cancer Res. 10 (10) (2020) 3370–3381.
[13] Q.-X. Meng, et al., ZNF384–ZEB1 feedback loop regulates breast cancer metastasis, Mol. Med. 28 (1) (2022) 111.
[14] H. Jiang, et al., Zeb1-induced metabolic reprogramming of glycolysis is essential for macrophage polarization in breast cancer, Cell Death Dis. 13 (3) (2022) 206.
[15] W. Li, et al., Insights into the post-translational modification and its emerging role in shaping the tumor microenvironment, Signal Transduct. Targeted Ther. 6 (1) (2021) 422.
[16] H. Wang, et al., Protein post-translational modifications in the regulation of cancer hallmarks, Cancer Gene Ther. 30 (4) (2023) 529–547.
[17] Y. Mizuguchi, et al., Cooperation of p300 and PCAF in the control of microRNA 200c/141 transcription and epithelial characteristics, PLoS One 7 (2) (2012) e32449.
[18] H.T. Wu, et al., Oncogenic functions of the EMT-Related transcription factor ZEB1 in breast cancer, J. Transl. Med. 18 (1) (2020) 51.
[19] Z. Zhou, et al., USP51 promotes deubiquitination and stabilization of ZEB1, Am. J. Cancer Res. 7 (10) (2017) 2020–2031.
[20] T. Narita, B.T. Weinert, C. Choudhary, Functions and mechanisms of non-histone protein acetylation, Nat. Rev. Mol. Cell Biol. 20 (3) (2019) 156–174.
[21] R.M. Gemmill, et al., ZEB1-responsive genes in non-small cell lung cancer, Cancer Lett. 300 (1) (2011) 66–78.
[22] J. Roche, et al., Global decrease of histone H3K27 acetylation in ZEB1-Induced epithelial to mesenchymal transition in lung cancer cells, Cancers (Basel) 5 (2) (2013) 334–356.
[23] J. Jin, et al., Oxidative stress-CBP axis modulates MOB1 acetylation and activates the hippo signaling pathway, Nucleic Acids Res. 50 (7) (2022) 3817–3834.
[24] M. Saito, et al., Acetylation of intrinsically disordered regions regulates phase separation, Nat. Chem. Biol. 15 (1) (2019) 51–61.
[25] R. Miao, et al., Gasdermin D permeabilization of mitochondrial inner and outer membranes accelerates and enhances pyroptosis, Immunity 56 (11) (2023) 2523–2541.e8.
[26] D. Chen, et al., Targeting oxidative stress-mediated regulated cell death as a vulnerability in cancer, Redox Biol. 84 (2025) 103686.
[27] C. Glorieux, et al., Targeting ROS in cancer: rationale and strategies, Nat. Rev. Drug Discov. 23 (8) (2024) 583–606.
[28] G. Lei, L. Zhuang, B. Gan, The roles of ferroptosis in cancer: tumor suppression, tumor microenvironment, and therapeutic interventions, Cancer Cell 42 (4) (2024) 513–534.
[29] A. Schwab, et al., Zeb1 mediates EMT/plasticity-associated ferroptosis sensitivity in cancer cells by regulating lipogenic enzyme expression and phospholipid composition, Nat. Cell Biol. 26 (9) (2024) 1470–1481.
[30] Z. Liu, et al., Multi-stage mechanisms of tumor metastasis and therapeutic strategies, Signal Transduct. Targeted Ther. 9 (1) (2024) 270.
[31] A. Akhmetkaliyev, et al., EMT/MET plasticity in cancer and go-or-grow decisions in quiescence: the two sides of the same coin? Mol. Cancer 22 (1) (2023) 90.
[32] Z. Li, et al., Tumour-associated macrophages enhance breast cancer malignancy via inducing ZEB1-mediated DNMT1 transcriptional activation, Cell Biosci. 12 (1) (2022) 176.
[33] N. Feldker, et al., Genome-wide cooperation of EMT transcription factor ZEB1 with YAP and AP-1 in breast cancer, EMBO J. 39 (17) (2020) e103209.
[34] P. Rosmaninho, et al., Zeb1 potentiates genome-wide gene transcription with Lef1 to promote glioblastoma cell invasion, EMBO J. 37 (15) (2018).
[35] W. Lehmann, et al., ZEB1 turns into a transcriptional activator by interacting with YAP1 in aggressive cancer types, Nat. Commun. 7 (2016) 10498.
[36] A.A. Postigo, et al., Regulation of smad signaling through a differential recruitment of coactivators and corepressors by ZEB proteins 22 (10) (2003) 2453–2462.
[37] E.C. Cheung, K.H. Vousden, The role of ROS in tumour development and progression, Nat. Rev. Cancer 22 (5) (2022) 280–297.
[38] D. Li, et al., Role of acetylation in doxorubicin-induced cardiotoxicity, Redox Biol. 46 (2021) 102089.
[39] H. Sies, R.J. Mailloux, U. Jakob, Fundamentals of redox regulation in biology, Nat. Rev. Mol. Cell Biol. 25 (9) (2024) 701–719.
[40] L. Xie, et al., Aspirin-mediated acetylation of SIRT1 maintains intestinal immune homeostasis, Adv. Sci. (Weinh.) 11 (19) (2024) e2306378.
[41] P. Sancho, D. Barneda, C. Heeschen, Hallmarks of cancer stem cell metabolism, Br. J. Cancer 114 (12) (2016) 1305–1312.
[42] C.L. Chaffer, et al., Poised chromatin at the ZEB1 promoter enables breast cancer cell plasticity and enhances tumorigenicity, Cell 154 (1) (2013) 61–74.
[43] D. Wang, et al., Zeb1-controlled metabolic plasticity enables remodeling of chromatin accessibility in the development of neuroendocrine prostate cancer, Cell Death Differ. 31 (6) (2024) 779–791.
[44] G. Lei, L. Zhuang, B. Gan, Targeting ferroptosis as a vulnerability in cancer, Nat. Rev. Cancer 22 (7) (2022) 381–396.